Valence-bond description of chemical reactions on Born–Oppenheimer molecular dynamics trajectories

Nao Noguchi[a] and Haruyuki Nakano[b]
Department of Chemistry, Graduate School of Sciences, Kyushu University, Fukuoka 812-8581, Japan

(Received 27 January 2009; accepted 19 March 2009; published online 17 April 2009)

The nature of chemical bonds on dynamic paths was investigated using the complete active space valence-bond (CASVB) method and the Born–Oppenheimer dynamics. To extract the chemical bond picture during reactions, a scheme to collect contributions from several VB (resonance) structures into a small numbers of indices was introduced. In this scheme, a tree diagram for the VB structures is constructed with the numbers of the ionic bonds treated as *generation*. A pair of VB structures is related to each other if one VB structure is transferred into the other by changing a covalent bond to an ionic bond. The former and latter VB structures are named *parent* and *child* structures, respectively. The weights of the bond pictures are computed as the sum of the CASVB occupation numbers running from the top generation to the bottom along the *descent* of the VB structures. Thus, a number of CASVB occupation numbers are collected into a small number of indices, and a clear bond picture may be obtained from the CASVB wave function. The scheme was applied to the hydrogen exchange reaction $H_2+F\rightarrow H+HF$ and the Diels–Alder reaction $C_5H_6(\text{cyclopentadiene})+CH_2=CH_2(\text{ethylene})\rightarrow C_7H_{10}(\text{norbornene})$. In both the reactions, the scheme gave a clear picture for the Born–Oppenheimer dynamics trajectories. The reconstruction of the bonds during reactions was well described by following the temporal changes in weight. © *2009 American Institute of Physics*. [DOI: 10.1063/1.3116787]

I. INTRODUCTION

To understand chemical reaction mechanisms it is important to obtain accurate potential energy surfaces (PESs) and to know the dynamics on them. At present, we have many accurate electronic structure theories for the PESs. The complete active space self-consistent field (CASSCF) method[1,2] is one of the electronic structure theories employed most frequently in the study of chemical reactions. This method is feasible and gives PESs of good quality, and is therefore also used as a starting point for higher-level multireference methods such as multireference configuration interaction, coupled cluster, and perturbation methods. In fact, the CASSCF method has many advantages for chemical reaction studies including (1) the well-defined potential energy surface of a chemical reaction if an appropriate active space is chosen, (2) its applicability to excited states as well as the ground state in a single framework, and (3) its provision of size-consistent results. Besides the electronic structure theories for PESs, the simulation methods for classical and quantum dynamics using PES have been well developed. In particular, as a classical dynamics method for isolated molecules, the Born–Oppenheimer (BO) dynamics method[3,4] has become a powerful tool. The BO dynamics method needs no potential functions fitted to the PESs and can use the energies and forces that are produced by *ab initio* electronic structure theories directly. Currently, the combination of the BO dynamics with the CASSCF method is a popular option because of the advantages (1)–(3) mentioned above, as well as the inexpensive force computation compared to other multiconfiguration-based methods that include the electron correlation effect.

In addition to the PESs and the dynamics on them, it is also crucial to obtain a clear picture for the reaction. In previous papers,[5,6] we have investigated chemical bond picture during reactions using the complete active space valence-bond (CASVB) method.[7–9] The CASVB method is a method that extracts a chemical picture from CASSCF wave functions. In this method, the CASSCF wave functions are transformed into the superpositions of VB (resonance) structures consisting of atomiclike orbitals without any loss of quality of the CASSCF wave function. The energies E_i^{CASSCF} and the densities $|\Psi_i^{\text{CASSCF}}|^2$ are unchanged in the transformation. Using this CASVB method, we examined collinear hydrogen exchange reactions $H_2+X\rightarrow H+HX$ (X=H, F, Cl, Br, and I) (Refs. 5 and 6) and a unimolecular dissociation $H_2CO\rightarrow H_2+CO$ (Ref. 5) on the intrinsic reaction coordinates (IRCs), and showed that the bond nature during the reactions is well analyzed with the occupation number of the VB structures.

However, the IRC is certainly a good reference reaction path for chemical reactions; it is a static path. The actual chemical reaction proceeds on a trajectory that is determined by the time evolution of the system, and it has been still unclear whether the CASVB may provide a good picture of bond breaking/formation along the dynamic trajectory, where the potential energies vary every moment and the system does not necessarily pass a transition state. Thus, in the present paper, we examine some chemical reactions on

[a]Present address: Pfizer Inc.
[b]Electronic mail: nakano@ccl.scc.kyushu-u.ac.jp.

Born–Oppenheimer trajectories using the CASVB method and discuss how the method describes the nature of the bonds during the reactions.

The contents of the present article are as follows. In Sec. II, after a brief survey of the CASVB method, we introduce a scheme by which we can organize many VB structures into a small number of indices. In Sec. III, the scheme is applied to the hydrogen exchange reaction $H_2+F\rightarrow H+HF$ and the Diels–Alder reaction $C_5H_6(\text{cyclopentadiene})+CH_2=CH_2(\text{ethylene})\rightarrow C_7H_{10}(\text{norbornene})$ on BO trajectories, and the applicability to the reactions is discussed. Conclusions are given in Sec. IV.

II. METHOD

A. Brief overview of the CASVB method

The CASVB method was proposed by Hirao *et al.*[7,8] They have proposed two versions of the CASVB method. The first one is a method to construct VB structures from orthogonal localized molecular orbitals (OLMOs), and the second is a method using nonorthogonal localized molecular orbitals (NLMOs). These methods provide different pictures of VB structures: a general feature is that the CASVB pictures with OLMOs have a more ionic nature than the pictures with NLMOs. An example is found in the hydrogen molecule. In the CASVB picture with OLMOs, the hydrogen molecule was described as a 61% covalent VB structure H–H and 39% ionic VB structure $H^+H^-+H^-H^+$, while the picture with NLMOs shows a 91% covalent and 9% ionic VB structure. However, as shown in a previous paper,[5] the bond pictures with both the sets of localized molecular orbitals (LMOs), which consist of the sum of the covalent and ionic VB structures, are very similar to each other. In the present article, therefore, we will use mainly a method with OLMOs, which may be treated more easily.

The idea of CASVB is based on the fact that the densities of variational wave functions are invariant under the transformations that hold the variational space unchanged. In the CASSCF case, the complete active space (CAS) is invariant under the linear transformation of active orbitals. We may redefine the active orbitals utilizing the invariance of the active orbital space. In the CASVB method with the OLMOs, the LMOs constructed by Boys' localization procedure[10] are used. If the active orbitals are defined appropriately, the LMOs nearly always turn out to be localized on a single atomic center with small localization tails onto neighboring atoms.

Let Ψ^{CASSCF} be a CASSCF wave function

$$\Psi^{\text{CASSCF}}=\sum_i C_i\Phi_i^{\text{CSF}},\quad \Phi_i^{\text{CSF}}\equiv\Phi_i^{\text{CSF}}(\{\varphi_i\}),\tag{1}$$

where Φ_i^{CSF} are the configuration state functions (CSFs) constructed by the orthogonal orbitals set $\{\varphi_i\}$ and C_i are the known CAS configuration interaction (CI) expansion coefficients. Similarly define the CASVB function in terms of spin-paired functions as

$$\Psi^{\text{CASVB}}=\sum_i A_i\Phi_i^{\text{VB}},\quad \Phi_i^{\text{VB}}\equiv\Phi_i^{\text{VB}}(\{\lambda_i\}),\tag{2}$$

where Φ_i^{VB} are spin-paired functions constructed with LMOs $\{\lambda_i\}$. The functions Φ_i^{VB} correspond to VB structures. The number of independent spin-paired functions is equal to the dimension of CAS. The spaces spanned by $\{\Phi_i^{\text{CSF}}\}$ and $\{\Phi_i^{\text{VB}}\}$ are identical. Because Eqs. (1) and (2) are different expressions of the identical wave function, we may write

$$\sum_j A_j\Phi_j^{\text{VB}}=\sum_j C_j\Phi_j^{\text{CSF}}.\tag{3}$$

Left-multiplying Eqs. (1) and (2) by Φ_i^{CSF} and integrating the products, we get a linear equation

$$\sum_j \Omega_{ij}A_j=C_i\quad\text{with}\quad \Omega_{ij}=\langle\Phi_i^{\text{CSF}}|\Phi_j^{\text{VB}}\rangle,\tag{4}$$

whose dimension is equal to the dimension of CAS. Solving this linear equation, we obtain CASVB wave function Ψ^{CASVB}. In the OLMO–CASVB case, we can use (Boys') LMOs $\{\lambda_i\}$ as $\{\varphi_i\}$ because the OLMOs remain CASSCF MOs. In that case, the linear equation (4) reduces to a set of linear equations for each orbital configuration, and the matrix Ω_{ij} for each linear equation becomes a triangular matrix depending only on spin configurations. The linear equation (4) can, therefore, be solved with ease, compared with the NLMO-CASVB case.

The occupation number of a VB structure is defined by

$$n_i=A_i^*\sum_j S_{ij}A_j,\tag{5}$$

where S_{ij} are overlaps between the VB structures i and j, defined by

$$S_{ij}=\langle\Phi_i^{\text{VB}}|\Phi_j^{\text{VB}}\rangle\tag{6}$$

and satisfies the normalization,

$$\sum_i n_i=1.\tag{7}$$

The occupation number represents the weight of a VB structure occupied in the CASVB, or equivalently CASSCF, wave function.

B. Tree diagram of VB structures with the number of ionic bonds used for *generation*

The CASVB occupation number is a good index to measure the contribution of each VB structure. However, the number of the VB structures is the same as the number of the CSFs in the CAS, which can grow large with the number of active orbitals. Even for CAS(6,6) for singlet states, appearing in the next section, includes 175 CSFs, where CAS(n,m) denotes the CAS made from n electrons by distributing them among m orbitals. It is therefore necessary to get together those many occupation numbers into a small number of other indices. In the present subsection, we introduce a scheme to do so.

The key idea is to arrange the VB structures treating the number of ionic bonds for *generation*. In the previous papers of the CASVB method,[7,8] we have shown the CASVB pic-

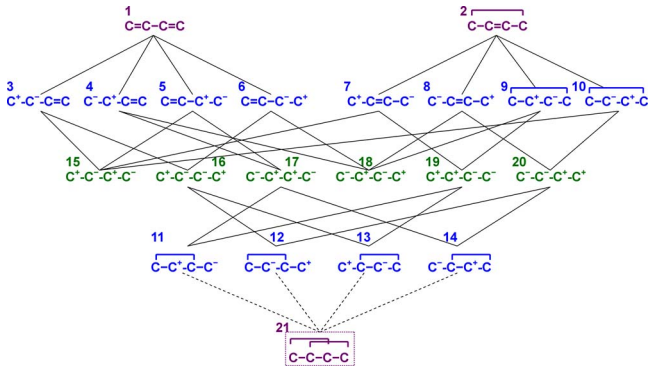

FIG. 1. (Color online) Tree diagram of the VB structures of butadiene. The VB structures in the first and fifth rows, in the second and fourth rows, and in the third row are the first-, second-, and third-generation VB structures, respectively. Structure 21 is a dummy covalent structure, which is not included in the CAS.

ture of butadiene (buta-1,3-diene). Let us take the VB structures of butadiene as an example. The butadiene has four π electrons and four π orbitals, which constitute CAS(4,4). The CAS(4,4) includes 20 CSFs or equivalently 20 VB structures (1–20) shown in Fig. 1. Structures 1 and 2 are covalent VB structures and hence have no ionic bonds. These VB structures belong to the first generation. Structure 1 generates structures 3–6 by changing a covalent bond into an ionic bond. Similarly, structure 2 generates structures 7–10. These VB structures have one ionic bond, hence, are in the second generation. We call structure 1 (2) *parent* structure of structures 3–6 (7–10), and inversely call structures 3–6 (7–10) *child* structures of structure 1 (2). Structures 11–14 cannot be generated from any VB structures by the change of a covalent bond to an ionic bond and hence do not have parent structures. The reason is that their parent structures have crossing covalent bonds, which are not allowed in CAS due to the linear dependency on the noncrossing-bond VB structures. Note that this exactly corresponds to the fact that the Rumer diagrams with crossing lines are linearly dependent on the diagrams without crossing lines.[11] However, if we add a covalent VB structure 21 with crossing bonds as a dummy structure, structure 11–14 can be generated from it. We call also structures 11–14 the second-generation VB structure although they have no real (namely, nondummy) parent structure. Structures 15–20, the third-generation VB structures, are generated from some of the second-generation VB structures. In this way, we can classify all the VB structures into generations according to the number of ionic bonds, and produce a tree diagram. In the same manner, we can construct a tree diagram for any CAS.

There are three VB structures, including the dummy VB structure, which do not have parent structures (the *root* structures). Because the child structures are generated by simply changing a bond from covalent to ionic, all the VB structures derived from these *root* structures have the same bonds. For example, structures 1, 3–6, and 15–18 all represent bonds C_1C_2 and C_3C_4 (hereafter we use bond structure $[C_1C_2, C_3C_4]$ for short). Similarly, structures 2, 7–10, and 15–20 represent bond structure $[C_1C_4, C_2C_3]$ and structures 11–14, 16, 17, 19, and 20 (and also dummy structure 21) represent bond structure $[C_1C_3, C_2C_4]$.

The total weight of a bond structure is defined by the sum of the weights of covalent, singly ionic, doubly, and higher ionic VB structures:

$$W_{\text{bond}} = w_{\text{covalent}} + w_{\text{singly ionic}} + w_{\text{doubly ionic}} + \cdots . \tag{8}$$

More concretely, the weight of bond structure $[AB, CD, \ldots]$ is defined by

$$\begin{aligned} W(AB,CD,\ldots) = {} & w(A-B,C-D,\ldots) + w(A^+B^-,C-D,\ldots) \\ & + w(A^-B^+,C-D,\ldots) + w(A-B,C^+D^-,\ldots) \\ & + w(A-B,C^-D^+,\ldots) + w(A^+B^-,C^+D^-,\ldots) \\ & + \cdots . \end{aligned} \tag{9}$$

If there is one-to-one correspondence between a parent and a child structure, we can use the occupation numbers n as the weights w in the right hand side. However, this is not always the case. If a child structure has more than one parent structure, the occupation number of the child structure is distributed in proportion to the occupation numbers of the parent structures:

$$w_{c\leftarrow p} = n_c f_{c\leftarrow p}, \quad f_{c\leftarrow p} = n_p / \left(n_p + \sum\nolimits_{p' \neq p} n_{p'} \right), \tag{10}$$

where $w_{c\leftarrow p}$ and $f_{c\leftarrow p}$ indicate the weight and fraction that is distributed to a parent structure p. If the parent structure has more than one grandparent structure, the weight is further distributed in the same manner:

$$w_{c\leftarrow p\leftarrow g} = n_c f_{c\leftarrow p} f_{p\leftarrow g}. \tag{11}$$

In other words, the weight w is a distributed occupation number depending on the occupation numbers of the root to parent structures.

Applying this scheme to butadiene, we have the weight of the bonds C_1C_2 and C_3C_4, for example,

$$\begin{aligned} W(C_1C_2,C_3C_4) &= w_1 + w_3 + w_4 + w_5 + w_6 + w_{15\leftarrow 3} + w_{15\leftarrow 5} + w_{16\leftarrow 3} + w_{16\leftarrow 6} + w_{17\leftarrow 4} + w_{17\leftarrow 5} + w_{18\leftarrow 4} + w_{18\leftarrow 6} \\ &= n_1 + n_3 + n_4 + n_5 + n_6 + n_{15}(f_{15\leftarrow 3} + f_{15\leftarrow 5}) + n_{16}(f_{16\leftarrow 3} + f_{15\leftarrow 6}) + n_{17}(f_{17\leftarrow 4} + f_{17\leftarrow 5}) + n_{18}(f_{18\leftarrow 4} + f_{18\leftarrow 6}) \\ &= n_1 + n_3 + n_4 + n_5 + n_6 + n_{15}\frac{n_3 + n_5}{n_3 + n_5 + n_7 + n_{10}} + n_{16}\frac{n_3 + n_6}{n_3 + n_6 + n_{12} + n_{13}} + n_{17}\frac{n_4 + n_5}{n_4 + n_5 + n_{11} + n_{14}} \\ &\quad + n_{18}\frac{n_4 + n_6}{n_4 + n_6 + n_8 + n_9}. \end{aligned} \tag{12}$$

The other weights, $W(C_1C_4,C_2C_3)$ and $W(C_1C_3,C_2C_4)$, are given similarly.

III. RESULTS AND DISCUSSION

A. Hydrogen exchange reaction, $H_2+F\rightarrow H+HF$

We first examine the hydrogen exchange reaction, $H_2+F\rightarrow H+HF$. This reaction is highly exothermic: the heat of the reaction is 30.8 kcal/mol. According to Hammond's postulate, this reaction should have an early TS. The PES and the dynamics of this reaction have been well examined.[12–14] What the electronic state is during this reaction and how the CASVB method describes the electronic structure, were examined on a static path, i.e., IRC, in a previous paper.[6] In the present paper, we examine how the CASVB method describes the chemical bond nature along dynamic paths, namely, the BO trajectories. We had trajectories with various initial conditions. Because our purpose is to show how the CASVB method presents the chemical bond nature, only several typical paths are shown. The algorithm of dynamics was the Verlet method with a time step of 0.5 fs. The classical equation of motion for the nuclei was integrated using the quantum mechanical forces for the CASSCF wave function, $F_i=-\nabla_i\langle\Psi_{\mathrm{CASSCF}}|H|\Psi_{\mathrm{CASSCF}}\rangle$.[15] Note that the BO dynamics paths of the CASVB and CASSCF methods are identical because the CASVB and CASSCF functions are different expressions of an identical wave function. The vibrational and rotational quantum numbers of the HF molecule were determined from trajectories employing the semiclassical Bohr–Sommerfeld quantization condition. The basis set used was Dunning's correlation-consistent polarized valence double zeta (cc-pVDZ) basis set.[16] Diffuse functions were augmented for fluorine.[17]

The active space was constructed by distributing three electrons in three orbitals consisting of $H_A(1s)$, $H_B(1s)$, and $F(2p\sigma)$, i.e., CAS(3,3). The dimension of the CAS is eight. According to this CAS, eight, linearly independent VB structures,

(1) $\varphi_{H_A}\varphi_{H_B}(\alpha\beta-\beta\alpha)\cdot\varphi_F\alpha$, H_A-H_B $F^{\bullet}$,
(2) $\varphi_{H_A}\alpha\cdot\varphi_{H_B}\varphi_F(\alpha\beta-\beta\alpha)$, $H_A^{\bullet}$ H_B-F,
(3) $\varphi_{H_B}\varphi_{H_B}(\alpha\beta-\beta\alpha)\cdot\varphi_F\alpha$, H_A^+ H_B^- $F^{\bullet}$,
(4) $\varphi_{H_A}\varphi_{H_A}(\alpha\beta-\beta\alpha)\cdot\varphi_F\alpha$, H_A^- H_B^+ $F^{\bullet}$,
(5) $\varphi_{H_A}\alpha\cdot\varphi_F\varphi_F(\alpha\beta-\beta\alpha)$, $H_A^{\bullet}$ H_B^+ F^-,
(6) $\varphi_{H_A}\alpha\cdot\varphi_{H_B}\varphi_{H_B}(\alpha\beta-\beta\alpha)$, $H_A^{\bullet}$ H_B^- F^+,
(7) $\varphi_{H_B}\alpha\cdot\varphi_F\varphi_F(\alpha\beta-\beta\alpha)$, H_A^+ $H_B^{\bullet}$ F^-, and
(8) $\varphi_{H_A}\varphi_{H_A}(\alpha\beta-\beta\alpha)\cdot\varphi_{H_B}\alpha$, H_A^- $H_B^{\bullet}$ F^+,

were used to construct CASVB functions. Here, in structures 1–8, the normalization constants and antisymmetrizers are omitted. According to the discussion in the previous subsection, the tree diagram for these VB structures is written as Fig. 2. In the figure, structure 9 is a dummy covalent VB structure. Because each child structure has only one parent structure, the total weights of the H_AH_B, H_BF, and H_AF bonds are simply given as the sum of the occupation numbers of the parent and child structures.

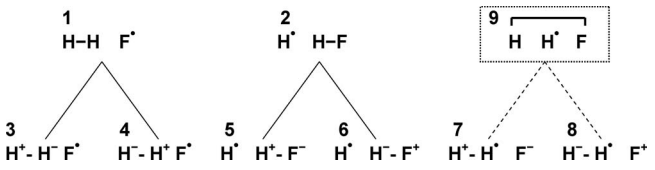

FIG. 2. Tree diagram of the VB structures for the H_A-H_B-F system. Structure 9 is a dummy covalent structure, which is not included in CAS(3,3).

$$W_{H_AH_B}=n_1+n_3+n_4, \tag{13}$$

$$W_{H_BF}=n_2+n_5+n_6, \tag{14}$$

$$W_{H_AF}=n_7+n_8. \tag{15}$$

First, we show the results of collinear reactions.

Figures 3(a)–3(d) are the results of the reaction where a fluorine atom with an initial kinetic energy, $E_K(F)=20.0$ kcal/mol, collides with a H_2 molecule in the ground vibrational state. The vibrationally excited HF molecule ($v=2$) was produced in this collision. Figures 3(a) and 3(b) show the changes in the z coordinates of the atoms (the z-axis was taken along the molecular axis of the H_2 molecule) and the potential energy, respectively. The changes in the coordinates and the potential energy in Figs. 3(a) and 3(b) show that the hydrogen exchange occurred during approximately $t=30-45$ fs. Figure 3(c) shows the changes of the occupation numbers of the covalent and ionic VB structures (two ionic VB structures, X^+Y^- and X^-Y^+, were collected into one structure), and the weights of the bonds were given from the occupation numbers by Eqs. (13)–(15), which were depicted in Fig. 3(d). The occupation numbers in Fig. 3(c) oscillate according to the vibrational motions of the H_2 and HF molecule. The phases of the oscillations are opposite for covalent and ionic VB structures in the noncollision region. Because both the H_2 and HF molecules undergo homolytic cleavage, their electronic structures are more covalent for the longer bond region and oppositely they are more ionic for the shorter bond region, which gives the opposite phase. Because of these oscillations, quantitative estimation of the contributions of the bonds is not a simple task at this stage. On the other hand, in Fig. 3(d) the exchange of the H_AH_B and H_BF bonds is clearly described. The weights of the H_AH_B (H_BF) bond began to decrease (increase) at around $t=25$ fs, and the two weights became equal at around $t=35$ fs, and subsequently a new H_BF bond was formed at around $t=50$ fs. The H_AF bond was small, as expected. The curves are very similar to those for the weights on the IRC in Ref. 6 except for the rebound at around $t=45$ fs, although the definition of the weight is slightly different.

Figures 4(a) and 4(b) illustrate the changes in the z-coordinates of the atoms and the potential energy for the reaction with an initial kinetic energy 12.7 kcal/mol. This is an example of nonreactive collisions. The changes of the occupation numbers and weights are shown in Figs. 4(c) and 4(d). The nonreactive feature was well represented in Fig. 4(d). In the collision time region, $t=30-60$ fs, the weight of the H_AH_B bond decreased to about 0.6 temporarily and that

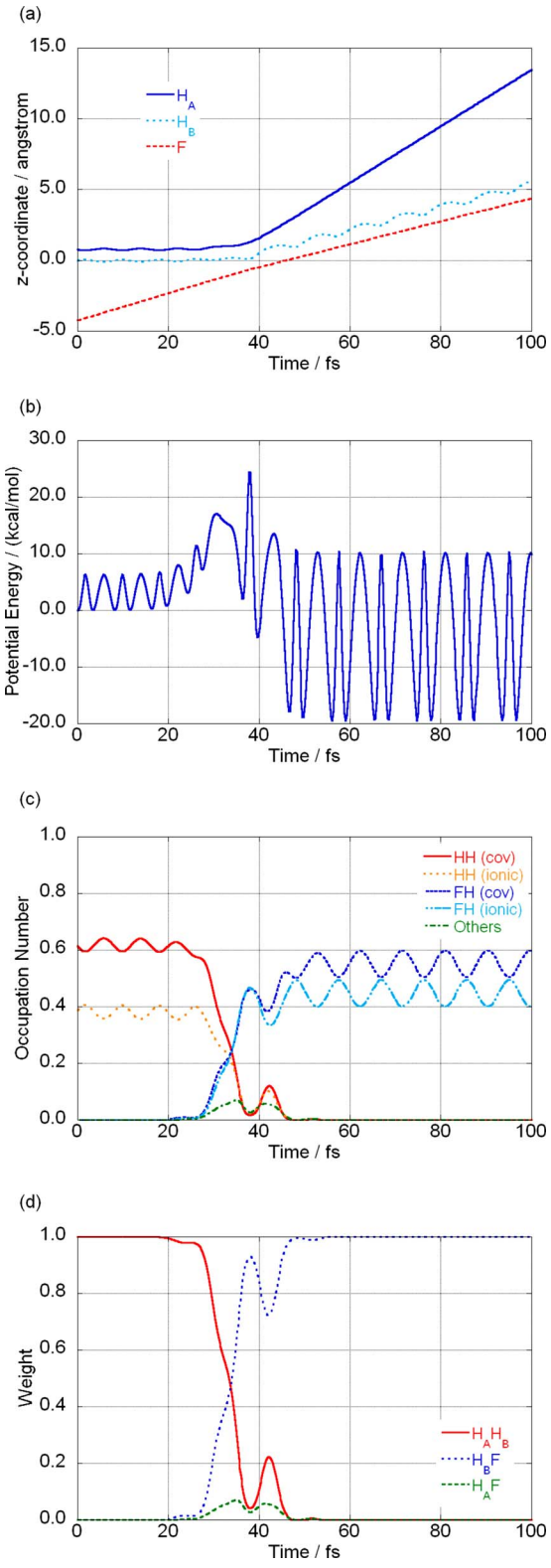

FIG. 3. (Color online) Results for a collinear reaction [E_K(F) =20.0 kcal/mol]: (a) Changes of the z-coordinates of the H_A, H_B, and F atoms for, (b) potential energy, (c) occupation numbers of VB structures, and (d) weights of bond structures.

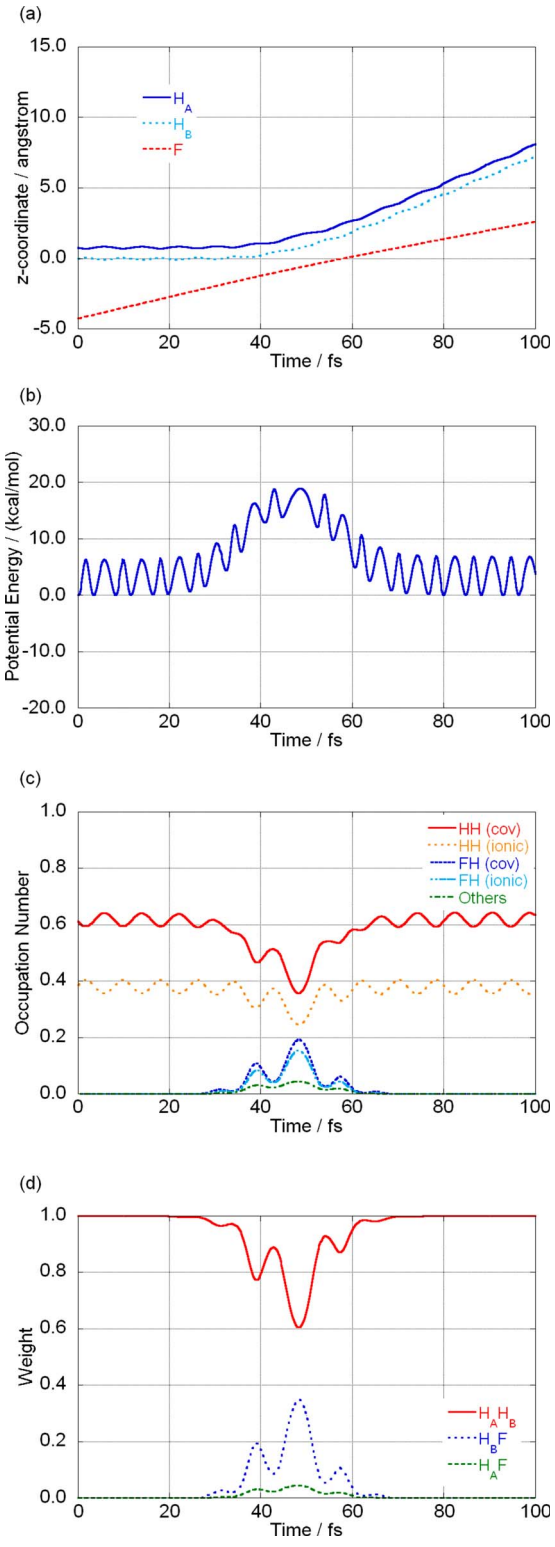

FIG. 4. (Color online) Results for a collinear reaction [E_K(F) =12.7 kcal/mol]: (a) Changes of the z-coordinates of the H_A, H_B, and F atoms, (b) potential energy, (c) occupation numbers of VB structures, and (d) weights of bond structures.

of the H_BF bond increased to about 0.35. However, after the collision time region, the weights returned to one and zero.

Subsequently, we show the results of noncollinear reactions. Figures 5(a)–5(d) are the results of the reaction where a fluorine atom with initial kinetic energy, E_K(F) =30.0 kcal/mol, collides with a H_2 molecule so that the incidence angle should be 30°. A vibrationally and rotationally excited HF molecule ($v=2$, $J=15$) was produced in this reaction. The exchanges of the z-coordinates of the H_B and F atoms in Fig. 5(a) represent the rotational motion of the HF molecule. The motions of the atoms were not simple com-

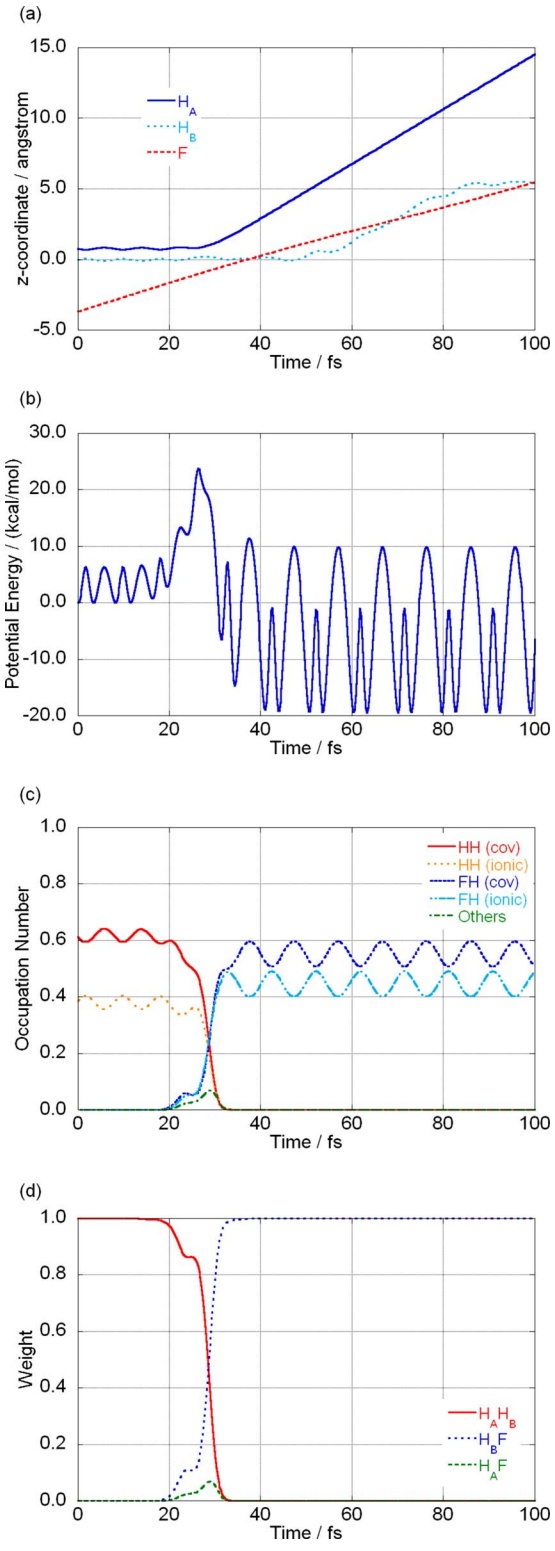

FIG. 5. (Color online) Results for a noncollinear reaction $[E_K(\mathrm{F})=30.0$ kcal/mol]: (a) Changes of the z-coordinates of the H_A, H_B, and F atoms, (b) potential energy, (c) occupation numbers of VB structures, and (d) weights of bond structures.

pared to the collinear reaction cases. However, it should be noted that, also in this noncollinear reaction case, the weights in Fig. 5(d) gave a clear picture, where the exchange of the bonds around $t=30$ fs is distinctly shown.

Finally, we show the CASVB results with NLMOs for the first collinear reaction $[E_K(\mathrm{F})=20.0$ kcal/mol] to compare them with the results of OLMOs. Figures 6(a) and 6(b) show the changes in the occupation numbers and the weights of the bonds, respectively. The occupation numbers of the CASVB methods with NLMO and OLMOs are rather different as can be seen from the comparison of Figs. 3(c) and 6(a). The ionic occupation number for NLMOs is smaller than that for OLMOs. In contrast, the weights of the bond in Figs. 3(d) and 6(b) are quite similar. These results, together with other examples in Ref. 5, support well the use of the weights of the bonds and OLMOs in the present article.

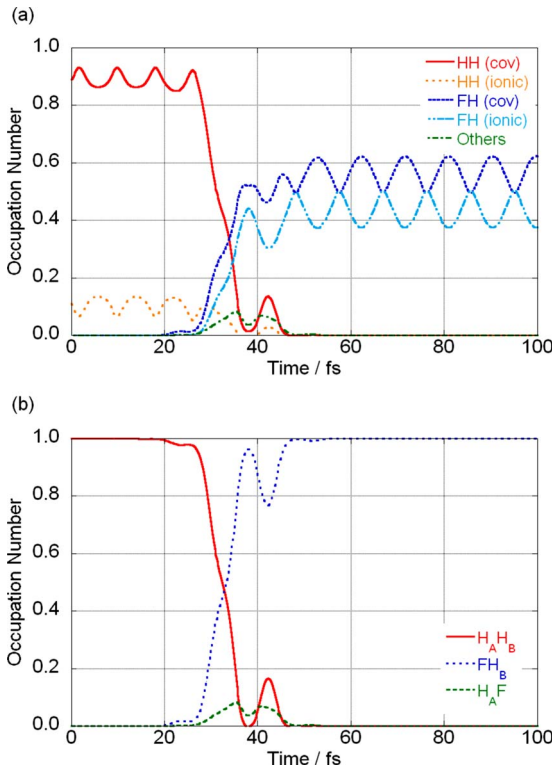

FIG. 6. (Color online) Results obtained with nonorthogonal localized molecular orbitals for the same reaction in Fig. 3: (a) occupation numbers of VB structures and (b) weights of bond structures.

B. Diels–Alder reaction C_5H_6(cyclopentadiene)+CH_2=CH_2(ethylene)→C_7H_{10}(norbornene)

The second example is the Diels–Alder reaction of cyclopentadiene (cyclopenta-1,3-diene) (referred to as CP hereafter) and ethylene (ethene) leading to the formation of norbornene (bicyclo[2.2.1]hept-2-ene) [referred to as NB hereafter].

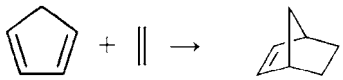

This reaction is a [4+2] cycloaddition reaction and widely known as a concerted reaction following the Woodward–Hoffman rule. The PES and dynamics of this reaction have been well studied by several groups. Houk and co-workers[18,19] examined the PES of this reaction and showed that the concerted path is the lowest path on the ground state surface. They also found a stepwise path that passes through a diradicaloid intermediate. Aktah *et al.*[20]

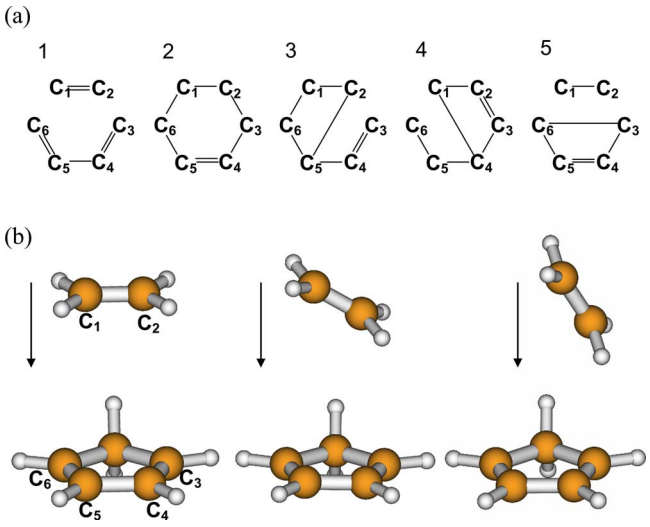

FIG. 7. (Color online) Diels–Alder reaction (CP+ethylene→NB): (a) numbering of the carbon atoms and five covalent VB structures, (b) three approaching paths (left: symmetric path; center and right: asymmetric path with an angle of skew of 30° and 60°, respectively).

conducted a dynamics study using Car–Parrinello molecular dynamics. Recently Hill *et al.* investigated the electronic rearrangement in the retro Diels–Alder reaction along the IRC using spin-coupled theory. They elucidated also the bonding nature along the IRC using the Chirgwin–Coulson weights and the Wiberg indices, which is closely related to the present study.[21] The purpose of this subsection is not to examine the reaction itself. We therefore focus on the CASVB picture of bond breaking/formation along some typical BO trajectories.

The active space used was CAS(6,6), where the four π orbitals of CP and the two π orbitals of ethylene were included in active orbitals. These six active orbitals correspond to four σ and two π orbitals of NB. The basis set used was the cc-pVDZ basis set.[16]

The CAS using six electrons and six orbitals includes 175 singlet CSFs, or equivalently, 175 VB structures. According to the scheme described in Sec. II A, we can construct a tree diagram for these VB structures. However, the tree diagram for this VB structure set is too complicated to be depicted in a figure, therefore, some features are described here.

Figure 7(a) shows the numbering of the carbon atoms in the system and five covalent VB structures. Numbered atoms C_1 and C_2 are the carbon atoms of ethylene, while C_3–C_6 are those of CP. These VB structures in Fig. 7(a) are in the first generation, from which 30 second-generation, 48 third-generation, and 20 fourth-generation VB structures are generated. In addition to these VB structures, there are 36 second-generation and 6 third-generation VB structures that correspond to crossing bonds such as [C_1C_2, C_3C_5, C_4C_6]. These VB structures do not have their parent covalent structures in the CAS for the same reason as mentioned in Sec. II B. Therefore, as parent structures of these crossing-bond VB structures, dummy (first-generation) covalent VB structures with crossing bonds are added to the tree diagram. More 36 third-generation VB structures are generated from the crossing-bond second-generation parent structures. Note that the 48 third-generation structures originating from the five covalent VB structures are also generated from the crossing-bond parent structures and that their occupation numbers are distributed according to the fraction described in Sec. II B.

Before seeing the weights on the BO trajectories, let us examine the weights in the reactants, the TS structure, and the product.

The weights in the reactant (the CP plus ethylene system) are as follows:

$$\text{Reactant: } 0.870[\text{I}] + 0.098[\text{V}] + 0.032[\text{CBs}]. \tag{16}$$

Here the [I]–[V] represent bond structures derived from the corresponding five covalent VB structures (root structures) 1–5 in Fig. 7(a) and [CBs] represents the set of all other bond structures that have crossing bonds. Note again the difference between the VB structure and the bond structure. For instance, structure 1 in Fig. 7(a) is a VB structure, while bond structure I is the aggregate of the VB structures with C_1C_2, C_3C_4, and C_5C_6 bonds. The numbers before bond structures in Eq. (16) express the weights with all the descendant occupation numbers put together. Equation (16) means that the reactant, the CP plus ethylene system, mainly consists of 87.0% of [C_1C_2, C_3C_4, C_5C_6] and 9.8% of [C_1C_2, C_3C_6, C_4C_5]. This immediately gives the fraction of [C_3C_4, C_5C_6] and [C_3C_6, C_4C_5] contribution in CP because ethylene is described by a single structure [C_1C_2].

The weights in the product (NB) and the TS structure are as follows:

$$\text{Product: } 0.001[\text{I}] + 0.923[\text{II}] + 0.018[\text{III}] + 0.018[\text{IV}] + 0.006[\text{V}] + 0.027[\text{CBs}], \tag{17}$$

$$\text{TS: } 0.262[\text{I}] + 0.291[\text{II}] + 0.095[\text{III}] + 0.095[\text{IV}] + 0.114[\text{V}] + 0.144[\text{CBs}]. \tag{18}$$

The product NB is almost described by [C_2C_3, C_4C_5, C_6C_1] (92.3%). The contributions from other four bond structures and crossing-bond bond structures are less than 3% each. The transition state is mainly described by a mixture of [C_1C_2, C_3C_4, C_5C_6] and [C_2C_3, C_4C_5, C_6C_1], the contribution of which is 26.2% and 29.1%, respectively. These contributions are close to each other, which indicates that the TS has a bond structure intermediate of the reactant's and of the

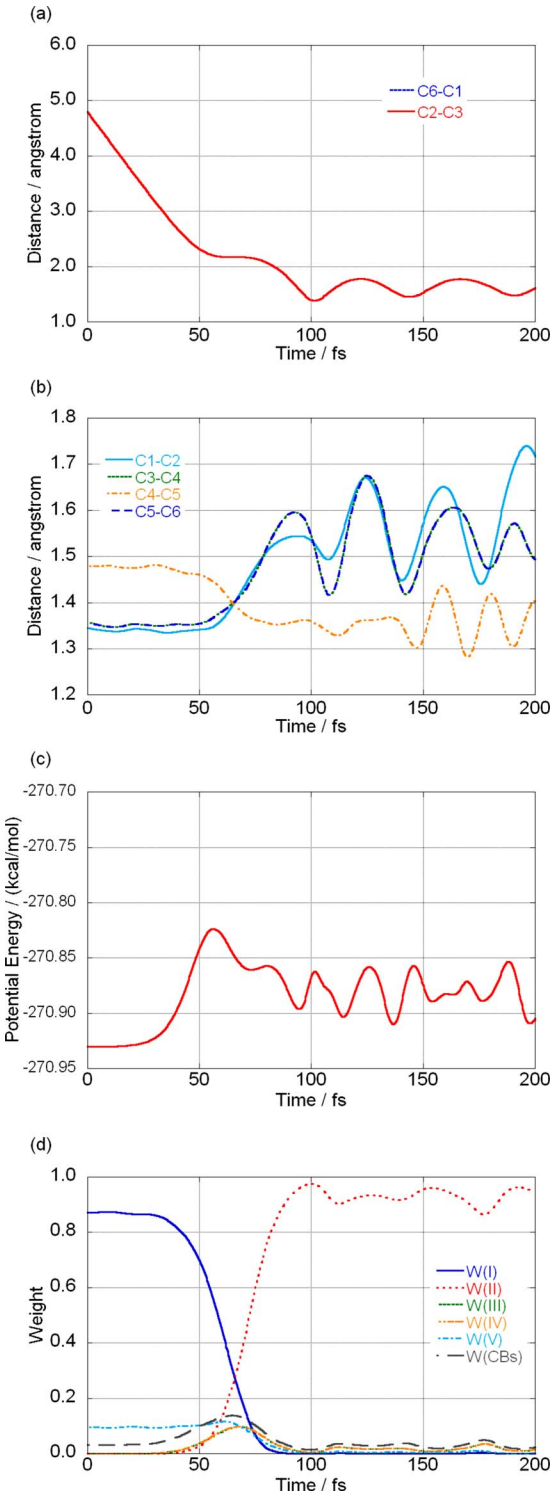

FIG. 8. (Color online) Results for an ideal symmetric path: (a) changes in the bond distances C_1-C_6, and C_2-C_3, (b) changes in the bond distances C_1-C_2, C_3-C_4, C_4-C_5, and C_5-C_6, (c) potential energy, and (d) weights of bond structures.

product's, though the weights of other bond structures are not very small. These results are consistent with our previous results.[5]

Then let us examine the bond picture on BO trajectories.

Figures 8(a)–8(d) show the results for an ideal symmetric trajectory with an initial ethylene kinetic energy of 100 kcal/mol [see Fig. 7(b)]. Here, the initial approaching path of ethylene was set so that the C_s symmetry of the system would be maintained and the $C_1C_2C_3C_6$ and CP plains would be perpendicular. Figure 8(a) shows the changes in bond distances between C_1 and C_6 and between C_2 and C_3, which are forming σ bonds between ethylene and CP. Figure 8(b) shows the changes of C_1C_2, C_3C_4, C_4C_5, and C_5C_6 bond distances, which are ethylene or CP intramolecular distances. In this case, the reaction proceeds concertedly owing to the symmetry restriction. Figure 8(a) indicates that the C_1C_6 and C_2C_3 bond formation was made at approximately $t=50-90$ fs and Fig. 8(b) indicates that the C_4C_5 bond changed from a single to a double bond and the C_3C_4 and C_6C_5 bonds from a double to single bonds at around $t=60$ fs. Figure 8(c) shows the change in the potential energy. The difference between the reactant system and the top of the curve was 66.8 kcal/mol, which was 25.1 kcal/mol larger than the activation energy. Figure 8(d) shows the bond picture along the trajectory. This figure clearly indicates rapid exchange of bond structures [C_1C_2, C_3C_4, C_5C_6] and [C_2C_3, C_4C_5, C_6C_1] (the C_1C_2, C_3C_4, and C_5C_6 double bonds to the C_2C_3 and C_6C_1 single and C_4C_5 double bonds) in a short time region $t=50-90$ fs. This picture, extracted from the electronic structure, was agreed well with the picture by the change of the bond lengths described in Figs. 8(a) and 8(b).

Figures 9(a)–9(d) are the results for an asymmetric initial condition with an initial ethylene kinetic energy of 150 kcal/mol [see Fig. 7(b)]. The initial configuration was constructed from the ideal C_s symmetry by slanting it by 30° (the $C_1C_2C_3C_6$ and CP planes were kept perpendicular). Figure 9(a), representing the changes of the C_1C_6 and C_2C_3 bond lengths, shows that bond lengths, which initially decreased at a constant rate, began to slowly oscillate at around $t=45$ and $t=75$ fs for C_2C_3 and C_1C_6 bonds, respectively and then oscillated together after $t=120$ fs. This behavior of bond lengths indicates C_1C_6 and C_2C_3 bond formation during $t=45-120$ fs. Figure 9(b) shows the changes of the same CC bonds as those in Fig. 8(b). Similar to Fig. 8(b), this figure shows the exchange of the single and double bonds at around $t=50$ fs. Figure 9(d) shows the change of the weights. This figure clearly shows the exchange of bond structures I and II, which is very similar to that in Fig. 8(d). A small difference is that bond structure III was a little larger than that in Fig. 8(d) at around $t=50$ fs. Bond structure III means only the C_6C_1 is bonded, not the C_2C_5; in other words, the nonconcerted portion contributed.

The last example also has an asymmetric initial condition. However, in this example the condition was set so that the C_2C_3 bond should be preferentially formed. The ethylene was initially placed so that its molecular plane and the CP plane made an angle of 60°, and in addition for the C_2C_3 line and CP plane to be perpendicular [see Fig. 7(b)]. Figures 10(a)–10(d) show the results for an initial ethylene kinetic energy of 250 kcal/mol. The changes in the bond lengths, Figs. 10(a) and 10(b), were similar to those of the previous two cases. From Fig. 10(b), the exchange of the single and double bonds appears to occur almost simultaneously at around $t=40$ fs. This observation is consistent with the bond picture in Fig. 10(d). This figure shows clearly the exchange

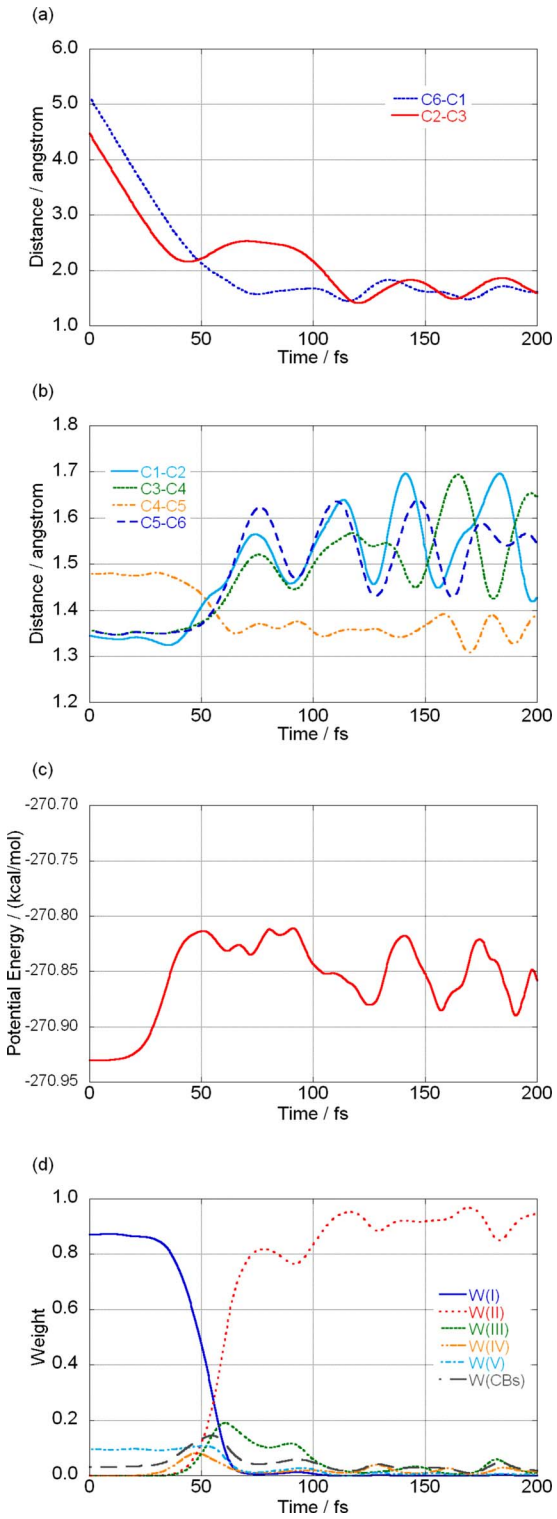

FIG. 9. (Color online) Results for an asymmetric path (angle of skew: 30°): (a) changes in the bond distances C_1-C_6, and C_2-C_3, (b) changes in the bond distances C_1-C_2, C_3-C_4, C_4-C_5, and C_5-C_6, (c) potential energy, and (d) weights of bond structures.

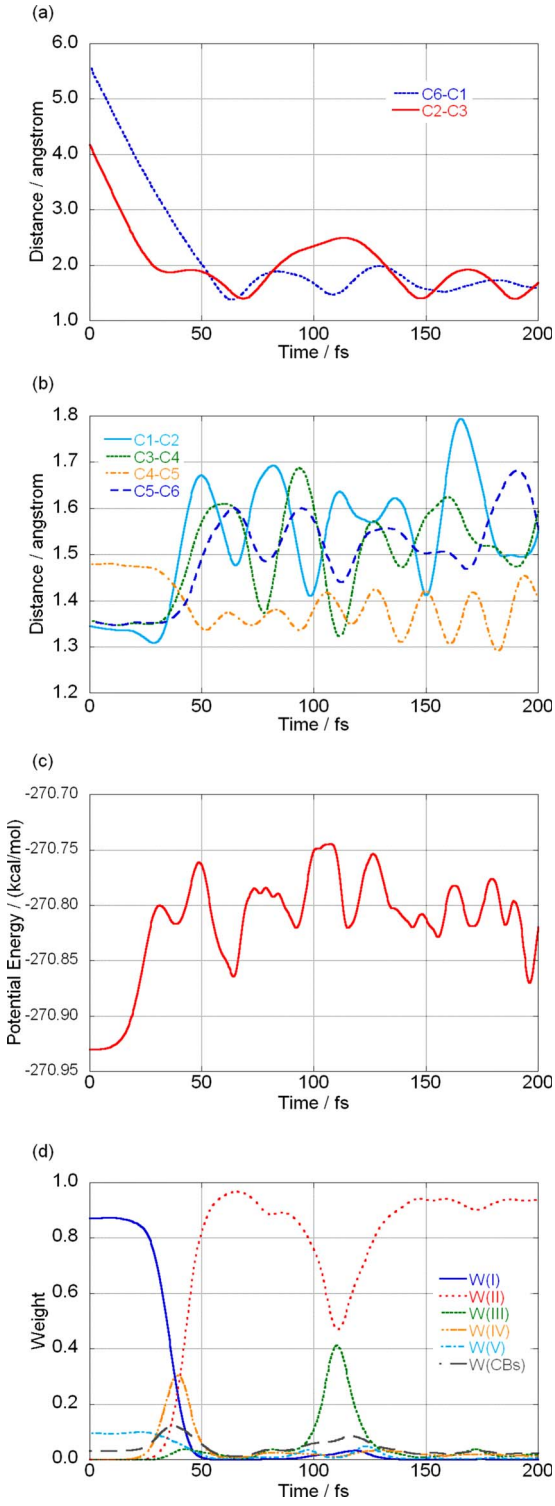

FIG. 10. (Color online) Results for an asymmetric path (angle of skew: 60°): (a) changes in the bond distances C_1-C_6, and C_2-C_3, (b) changes in the bond distances C_1-C_2, C_3-C_4, C_4-C_5, and C_5-C_6, (c) potential energy, and (d) weights of bond structures.

of the bond structures I and II, namely, the [C_1C_2, C_3C_4, C_5C_6] to [C_2C_3, C_4C_5, C_6C_1] concerted change. On the reflection of the biased condition for the C_2C_3 bond, bond structure IV, which means mainly the C_2C_3 bond, occurred for a very short time in the exchange time region.

A feature in this graph is the elevation of bond structure III and the fall of bond structure II at around $t=110$ fs. This can be explained by the large changes in some CC bond lengths. Around this time, the C_2C_3 bond length temporarily increased to about 2.5 Å because of the repulsion caused by the collision to the CP plane. At the same time, the C_3C_4 bond length became near double by oscillation. These changes increased the contribution of bond structure III and decrease that of bond structure II. However, the other bonds

remained near the bond lengths of NB; thus, the contribution of bond structure II becomes dominant again. A similar, but smaller change can be also seen in Fig. 9(d) at around $t = 90$ fs.

Finally, to obtain deeper insight into the electronic structures during reactions, we introduce *distance* between the bond structures at geometries X and Y,

$$d_{X-Y} = \max(|W_{\mathrm{I}}(X) - W_{\mathrm{I}}(Y)|,\ |W_{\mathrm{II}}(X) - W_{\mathrm{II}}(Y)|, |W_{\mathrm{III}}(X) - W_{\mathrm{III}}(Y)|,\ |W_{\mathrm{IV}}(X) - W_{\mathrm{IV}}(Y)|, |W_{\mathrm{V}}(X) - W_{\mathrm{V}}(Y)|,\ |W_{\mathrm{CBs}}(X) - W_{\mathrm{CBs}}(Y)|), \quad (19)$$

defined with the weights at X and Y (namely, $W_A(X)$ and $W_A(Y)$, respectively). This is a simple measure of the difference of electronic structures expressed by the weights between two different geometries. However, because weights include only reduced information of the original electronic structures, it should be noted that $d_{X-Y}=0$ does not necessarily indicate that the electronic structures at X and Y are identical. Figures 11(a)–11(c) are the plots of the changes of three distances $d_{\text{Z-R}}$, $d_{\text{Z-TS}}$, and $d_{\text{Z-P}}$ for the three different initial conditions discussed in the present subsection. Here Z is the geometry at a time and R, TS, and P stand for the geometries of the reactant, transition state, and product, respectively. The three figures clearly show that the electronic structure of the system was changed from that of the reactant to that of the product rapidly, not passing through other types of electronic structure. The time of the reaction was about 50–150 fs. These indicate that, in all the cases examined, the reaction proceeded concertedly.

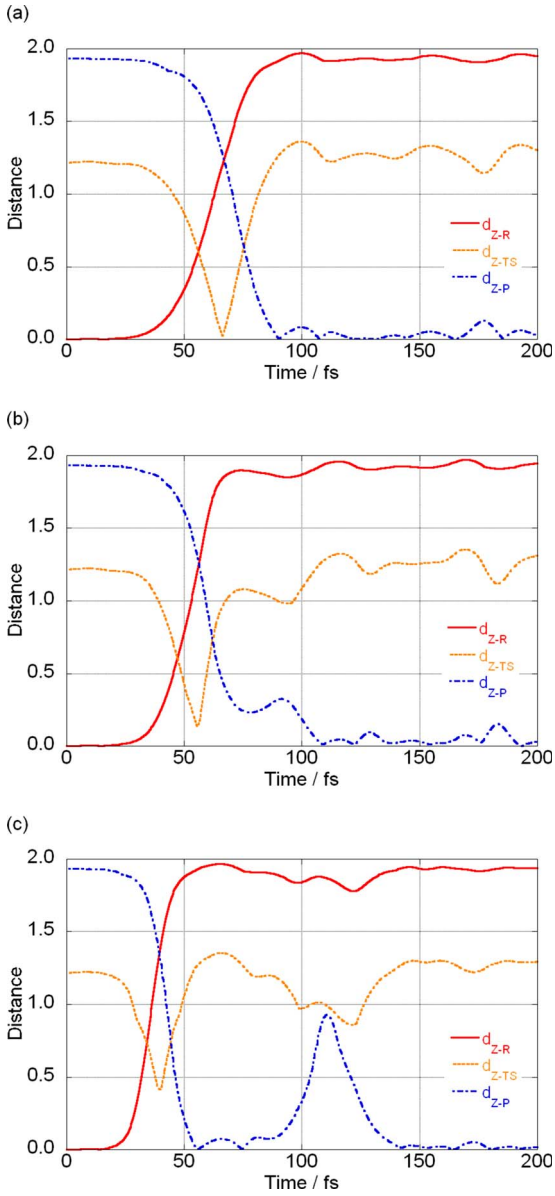

FIG. 11. (Color online) Distances from the reactant, TS structure, and product bond structures: (a) symmetric path, (b) asymmetric path (angle of skew: 30°), (c) asymmetric path (angle of skew: 60°).

IV. CONCLUSIONS

In the present article, we investigated the nature of chemical bond on dynamic paths using the CASVB method and BO dynamics. To extract the chemical bond picture during dynamics, we introduced a scheme to collect the contributions from several VB structures into small numbers of indices. In this scheme, first we make a tree diagram by arranging the VB structures using the numbers of their ionic bonds for *generation*. A pair of VB structures is related to each other if one VB structure has a covalent bond in a bond and another VB structure has an ionic bond in the same bond and, in addition, all the other bonds have the same type of bonds. We named the former a *parent* structure and the latter a *child* structure. Subsequently, using the tree diagram, we computed the weights of the bond structure by the summation of the CASVB occupation numbers. This summation runs from the top generation to the bottom along the descent. If a child structure has more than one parent, the occupation numbers of the children are distributed according to the occupation numbers of the parents.

We applied the scheme to the hydrogen exchange reaction $H_2+F \rightarrow H+HF$ and the Diels–Alder reaction $C_5H_6(\text{cyclopentadiene})+CH_2=CH_2(\text{ethylene}) \rightarrow C_7H_{10}(\text{norbornene})$. In both the reactions, the scheme gave a clear picture even for the BO dynamics trajectories. The graphs of the weights of the bonds showed that the reconstruction of chemical bonds during reactions could be viewed quantitatively by the temporal change of weight. We believe that CASVB weight analysis combined with BO dynamics is a useful tool for understanding chemical reaction mechanisms.

ACKNOWLEDGMENTS

This work was partly supported by the CREST of the Japan Science and Technology Agency (JST).

[1] K. Ruedenberg, L. M. Cheung, and S. T. Elbert, Int. J. Quantum Chem. **16**, 1069 (1979).
[2] B. O. Roos and P. R. Taylor, Chem. Phys. **48**, 157 (1980).
[3] T. Helgaker, E. Uggerud, and H. J. A. Jensen, Chem. Phys. Lett. **173**, 145 (1990).
[4] E. Uggerud and T. Helgaker, J. Am. Chem. Soc. **114**, 4265 (1992).
[5] H. Nakano, K. Nakayama, and K. Hirao, J. Mol. Struct.: THEOCHEM **461–462**, 55 (1999).
[6] H. Nakano, K. Sorakubo, K. Nakayama, and K. Hirao, in *Valence Bond Theory, Theoretical and Computational Chemistry*, edited by D. L. Coo-

per (Elsevier, Amsterdam, 2001), Vol. 10.
[7] K. Hirao, H. Nakano, K. Nakayama, and M. Dupuis, J. Chem. Phys. **105**, 9227 (1996).
[8] K. Hirao, H. Nakano, and K. Nakayama, J. Chem. Phys. **107**, 9966 (1997).
[9] Thorsteinsson *et al.* also investigated the transformations of CASSCF functions to modern valence-bond representations [T. Thorsteinsson, D. L. Cooper, J. Gerratt, P. B. Karadakov, and M. Raimondi, Theor. Chim. Acta **93**, 343 (1996)]. This method was also named the "CASVB method."
[10] J. M. Foster and S. F. Boys, Rev. Mod. Phys. **32**, 300 (1960).
[11] R. Pauncz, *Spin Eigenfunctions: Construction and Use* (Plenum, New York, 1979).
[12] C. F. Bender, S. V. O'Neil, P. K. Pearson, and H. F. Schaefer III, Science **176**, 1412 (1972).
[13] D. W. Schwenke, R. Steckler, F. B. Brown, and D. G. Truhlar, J. Chem. Phys. **84**, 5706 (1986).
[14] H.-J. Werner, M. Kállay, and J. Gauss, J. Chem. Phys. **128**, 034305 (2008), and references therein.
[15] Z. Liu, L. E. Carter, and E. A. Carter, J. Phys. Chem. **99**, 4355 (1995).
[16] T. H. Dunning, Jr., J. Chem. Phys. **90**, 1007 (1989).
[17] R. A. Kendall, T. H. Dunning, Jr., and R. J. Harrison, J. Chem. Phys. **96**, 6796 (1992).
[18] B. R. Beno, S. Wilsey, and K. N. Houk, J. Am. Chem. Soc. **121**, 4816 (1999).
[19] S. Wilsey, K. N. Houk, and A. H. Zewail, J. Am. Chem. Soc. **121**, 5772 (1999).
[20] D. Aktah, D. Passerone, and M. Parrinello, J. Phys. Chem. A **108**, 848 (2004).
[21] J. G. Hill, D. L. Cooper, and P. B. Karadakov, J. Phys. Chem. A **112**, 12823 (2008).